Check for updates

Computational fluid dynamics modelling of quasi-collimated beam apparatus – a typical bench scale UV apparatus for water treatment

Junfeng Lian, Liangmin Sun, Chong Jiang, Wentao Li, Yichun Zhu, Xinxin Qin and Zuwen Liu

ABSTRACT

Quasi-collimated beam apparatus (QCBA), a typical bench scale UV apparatus, is crucial for the biodosimetry determination of UV dose in target reactors. However, the key parameters for the QCBA construction are usually estimated via rule-of-thumb calculations. Computational fluid dynamics models are applied in this study to simulate the UV fluence rate (FR) distributions in QCBAs. QCBAs with either a cylindrical tube or successive apertures irradiate quasi parallel light into selected dishes. The simulated Petri factors (PF) in the target QCBAs with a single aperture were all >0.84, and increased with the extended distance (L_1) from the UV lamp to the upper aperture. QCBAs with two successive apertures are recommended compared with those with three apertures or cylindrical tube. A trend of FR distribution from dispersed to concentrated is observed when L_1 or the interval distance between each aperture increases in a dual-aperture QCBA. QCBAs with multiple lamps were favorable to increase the UV output power, while having a nearly negligible loss of parallelism. An actual QCBA was constructed, and the maximal and average FR and PF values in a 60-mm dish were 0.159 and 0.164 W/m^2, and 0.967, respectively, in accordance with the simulated results.

Key words | computational fluid dynamics, Petri factor, quasi-collimated beam apparatus, UV fluence rate

Junfeng Lian (corresponding author)
Liangmin Sun
Chong Jiang
Yichun Zhu
Xinxin Qin
Zuwen Liu
Ganzhou Key Laboratory of Basin Pollution Simulation and Control,
Jiangxi University of Science and Technology,
Ganzhou 341000,
China
E-mail: *lianjf@jxust.edu.cn*

Wentao Li
Key Laboratory of Drinking Water Science and Technology,
Research Center for Eco-Environmental Sciences,
Chinese Academy of Sciences,
Beijing 100085,
China

HIGHLIGHTS

- The designed collimator diameter should be larger than the reactor diameter.
- FR distributions transformed from dispersed to concentrated when the distance between the lamp and the collimator increased.
- QCBAs with two successive apertures were enough to produce satisfactory parallel beams.
- QCBAs with multiple lamps were favorable to increase the UV output power with a nearly negligible loss of parallelism.

This is an Open Access article distributed under the terms of the Creative Commons Attribution Licence (CC BY-NC-ND 4.0), which permits copying and redistribution for non-commercial purposes with no derivatives, provided the original work is properly cited (http://creativecommons.org/licenses/by-nc-nd/4.0/).

doi: 10.2166/wst.2021.144

Downloaded from http://iwaponline.com/wst/article-pdf/83/10/2526/892299/wst083102526.pdf
by guest

GRAPHICAL ABSTRACT

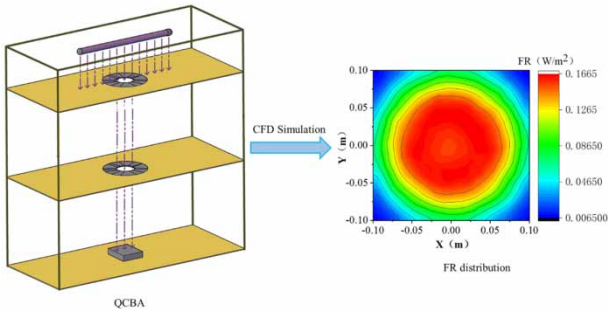

INTRODUCTION

Ultraviolet (UV) light has been applied worldwide for disinfection of water and wastewater (Spiliotopoulou *et al.* 2015; Zhang *et al.* 2019; Ao *et al.* 2020), owing to advantages such as high efficiency, broad antibacterial spectrum, minimal disinfection byproducts, easy maintenance and operation, and small equipment size. The number of drinking water plants in China that applied UV for disinfection was more than 1,500 in 2016, and more than half of the existing wastewater treatment plants applied UV disinfection as an effective barrier against viral pathogens, with the regulated minimum UV dose of 40 and 20 mJ/cm^2 for drinking water and wastewater disinfection (GAQSIQ 2005), respectively. To regulate the design and application of UV disinfection equipment utilized in water and wastewater treatment plants, a series of national standards have been issued in China, for example, GB/T19837-2005 (GAQSIQ 2005) and GB50014-2006 (MOHURD 2006).

Accurate assessment of UV dose for target UV equipment is of great significance. Manufacturers require precise and objective evaluation of their products for quality control. Water and wastewater treatment plants and supervision authorities also require short- or long-term monitoring of the applied UV equipment to guarantee long-lasting and stable efficiency, especially for the reason that UV fluence rate (FR) would attenuate with aging of UV lamps (Schmalwieser *et al.* 2014) and fouling of quartz sleeves (Lebedev *et al.* 2019).

At present, a rapid and accurate measurement of UV dose is still a challenging problem in the field of UV disinfection, and has restricted the further application of UV disinfection technology. Biodosimetry (Qualls & Johnson 1983) is a commonly admitted standard method for the measurement of UV dose in UV disinfection reactors, which applies nonpathogenic microorganisms (e.g., *MS2 coliphage* and *colibacillus*) as models. For example, in China a detailed protocol for the biodosimetry determination of UV dose was regulated (GAQSIQ 2005), and different model microorganisms were recommended in various cases (i.e., *colibacillus* for wastewater system, *MS2 coliphage* for drinking water system, and *MS2 coliphage* and *colibacillus* synergistically for reclaimed water system). A UV dose-response curve is vital for the biodosimetry determination of UV dose, which reflects the positive correlation between UV dose and inactivation efficiency. Quasi-collimated beam apparatus (QCBA) is the only admitted system to obtain the UV dose-response curve. In addition, QCBA facilitates obtaining an FR value quickly and accurately, using a radiometer and a corresponding equation (Bolton *et al.* 2015). Thus, it is widely utilized for the study of UV disinfection (Ke *et al.* 2009), photochemical processes (Stefan & Bolton 2005), and UV-based advanced oxidation processes, such as UV/H_2O_2, UV/chlorine, and UV photocatalysis (Baeza & Knappe 2011; Jin *et al.* 2011; Jefferson *et al.* 2016).

However, to the best of our knowledge, there are no clear guidelines or norms for the construction of QCBAs, and the key parameters are usually estimated via rule-of-thumb calculations. In China, there is scarcely any mass-production of QCBAs at present, and most of the customized products possess some shortcomings, e.g., low output intensity and insufficient parallelism of the UV beam. Lian *et al.* (2015) studied the UV photolysis kinetics of sulfonamides using a QCBA system monitored with a micro-fluorescent silica detector; the average irradiance in the applied QCBA was less than 0.1 mW/cm^2, and the parallelism was quite weak with a low Petri factor (PF) of $<$0.80, which is defined as the average ratio of the

Downloaded from http://iwaponline.com/wst/article-pdf/83/10/2526/892299/wst083102526.pdf
by guest

radiometer readings on the selected points (usually one point every 5 mm horizontally and vertically) over the area of the selected reactor (Petri dish in general) to the radiometer reading at the center of the selected reactor, applied to correct for the horizontal divergence of UV beam.

Computational fluid dynamics (CFD) has been widely applied in the design of UV reactors (Sozzi & Taghipour 2006; Sultan 2016; Pan *et al.* 2020). Therefore, this study was aimed to: (1) simulate and assess the QCBA performance using CFD; (2) study the effect of different factors that control the output intensity and parallelism of UV beam, including the collimator types (cylindrical tube or successive apertures), the number and position of apertures, and the number and arrangement of UV lamps; (3) optimize the design parameters of QCBA and verify its performance in practice. This study would promote the standardization of QCBA production and the precise quantification of UV dose.

MATERIALS AND METHODS

QCBA configurations

Two commonly applied QCBA configurations, with different collimator types, were studied, as illustrated in Figure 1. The main configurations included apparatus frames and walls, ballast, UV lamps and lamp holders, reactor (Petri dish in this paper) platform, and collimators. The collimator, either cylindrical tube or successive apertures, could induce a large ratio of the distance (L) between the lamp and the Petri dish to the practical lamp length (l), which refers to the length of UV lamp section whose beams can efficiently irradiate the target dish. In this situation, QCBAs could be considered as point sources, and UV beams from these point sources could be evenly distributed over the dish surfaces.

In general, the diameters of selected Petri dishes used as reactors in QCBAs are less than 100 mm. Thus, in this paper, the collimator diameter (D) of simulated QCBAs was fixed at 100 mm, and the dish diameters (d) were set as 60, 80, and 100 mm, respectively. The UV lamp was set in a lamp holder vertically above the collimator. The lamp power was set as 10 W with a UVC efficiency of 30% (except for the simulations of different irradiations). The arc length was fixed at 135 mm, and the lamp sleeve was 15 mm in diameter, as per an actual BOS-1T5 UVC lamp (Comwin, Foshan, Guangdong, China) and the matched sleeve. In order to maintain beam parallelism, the distance from the sample to the UV lamp is suggested to be set to at least four times the D value (Bolton & Stefan 2002), and in this study, the core of the lamp was 900 mm away from the top surface of the reaction solution in a target Petri dish. To avoid a large skewness in the following meshing process, the thickness of the collimator was set as 10 mm, which had little influence on the simulation results.

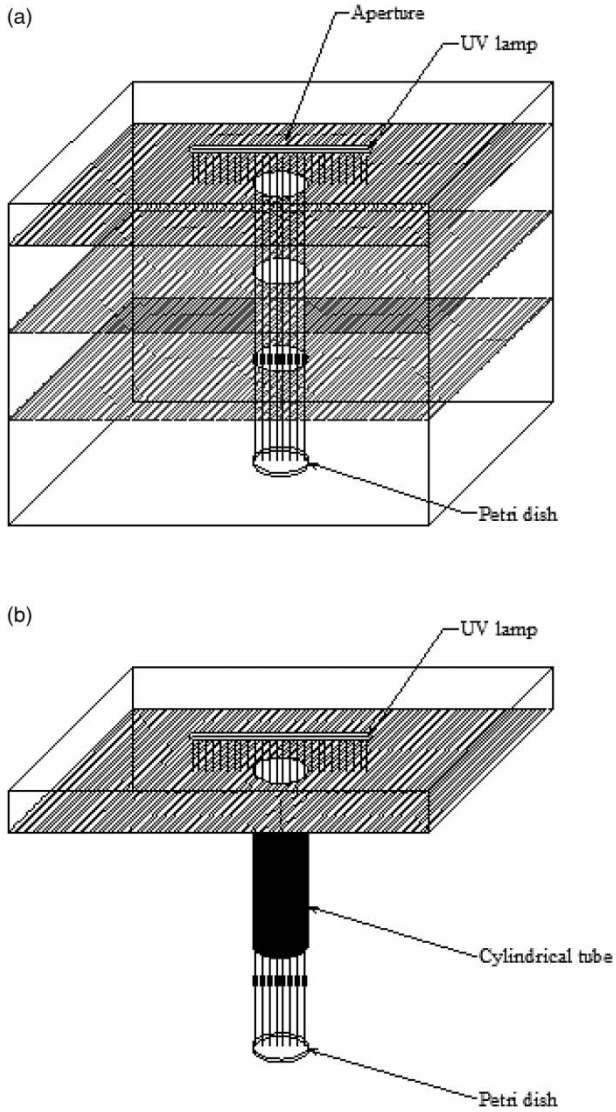

Figure 1 | Schematic diagram of two modelled QCBAs: (a) successive apertures type, and (b) cylindrical tube type.

CFD model settings

The simulation of QCBA was performed via the FLUENT component in a commercial CFD software package (ANSYS FLUENT 13.0, Canonsburg, PA, USA), which has been widely applied for the reliable simulation of FR

Downloaded from http://iwaponline.com/wst/article-pdf/83/10/2526/892299/wst083102526.pdf
by guest

distributions in UV reactors (Li *et al.* 2016, 2017). A tetrahedrons method using a patch conforming algorithm was applied for the meshing of CFD geometry. The QCBA inwall and the lamp sleeve were smoothly inflated for the relatively huge variations of the light field in these areas. The maximum mesh size was less than 10 mm, resulting in more than 1 million cells with the average skewness less than 0.25 (detailed in Figure S1, Supplementary Material). These meshes could ensure a mesh-independent simulation, and further increasing the number of cells made little difference.

A pressure-based solver and discrete ordinates (DO) radiation model were employed to simulate the FR distributions in designed QCBAs. The DO model could be expressed as follows (Gholamalizadeh & Kim 2014):

$$\nabla \cdot (I_\lambda(\vec{r}, \vec{s})\vec{s}) + (\alpha_\lambda + \sigma_s)I_\lambda(\vec{r}, \vec{s}) = \alpha_\lambda n^2 I_{b\lambda}\frac{\sigma_s}{4\pi}\int_0^{4\pi} I_\lambda(\vec{r}, \vec{s})\Phi(\vec{s}, \vec{s'})d\Omega' \quad (1)$$

where $\alpha_\lambda + \sigma_s =$ optical thickness or opacity of the medium; $\alpha_\lambda =$ spectral absorption coefficient; $I_{b\lambda} =$ black body intensity given by the Planck function. The boundary condition on the lamp sleeve was set to be semi-transparent type, and the direct irradiation (E_o, W/m^2) was calculated via Equation (2):

$$E_0 = \frac{P\eta}{A} \quad (2)$$

where $P =$ lamp power (W), $\eta =$ UVC efficiency of the target lamp (30% in this study), and $A =$ surface area of the lamp sleeve (m^2). In addition, to minimize the influence of blackbody emission, the initial temperature of the simulated lamp was set at 3 K. The pressure-velocity coupling scheme was set as SIMPLE method, and the spatial discretization methods of gradient and pressure were set as node based Green-Gauss and standard method, respectively; spatial discretization methods for all other parameters were set as second order upwind method. Solutions were considered to be convergent when the normalized residual was $<10^{-5}$. FR (average and maximal values) and PF values on the upper surface of a given Petri dish were utilized to assess the performance of simulated QCBAs.

Model verification

To verify the CFD simulation results, an actual QCBA with optimal parameters was constructed and tested (Figure S2). The frames of the constructed QCBA were fabricated from angle iron and the walls were made of 5-mm-thick acrylic plates. To minimize UV reflection, upper surfaces of walls next to the collimator were coated with black UV-absorbing materials. A ventilation system was installed in the upper room to avoid variations of output light intensity caused by continuous heating of UV lamps. For ease of movement, the four feet were also equipped with universal wheels and brake pads. FR values in the constructed QCBA were determined with a radiometer (UV-B, Photoelectric Instrument Factory of Beijing Normal University, Beijing, China), which was annually calibrated by the National Institute of Metrology (Beijing, China), and PF values were determined according to previous studies (Bolton & Linden 2002; Bolton *et al.* 2015).

RESULTS AND DISCUSSION

UV beams constrained by one single aperture

Figure S3 and Figure 2 show the simulated FR distributions and the related FR and PF values on target surfaces induced by beams constrained by a single aperture. The central point did not always have the largest FR value, especially in QCBAs with dispersive beams (e.g., in Figure S3(a) and S3(b)). In this study, the term PF is redefined as the ratio of average FR to the maximum value in the target area.

Irradiation from the simulated QCBAs with one single aperture was possessed of a certain parallelism, with PF values > 0.84. As the distance (L_1) from the UV lamp to the upper aperture extended, an increasing PF and FR value could be observed (the maximal and average FR value and PF value in a 100-mm dish increased by 25.6, 40.2, and 11.5%, respectively, when L_1 increased from 100 to 600 mm). A transformation of FR distribution was also shown from dispersion to concentration along the direction of the lamp.

As illustrated in Figure S4, scenarios of UV irradiation in all directions could be simplified as a successive transition from scenario I (view along the lamp, shown in Figure S4(a)) to scenario II (view normal to the lamp, shown in Figure S4(b)), and in this transition, the function of aperture becomes important. In scenario II with the assumption of $D = d$, according to the geometric law, the l value was equal to $D \times (L + L_1)/(L - L_1)$, and the minimum included angle (α) between UV beam and Petri dish surface was equal to arctan $[(L - L_1)/D]$. On the one hand, an extended L_1 meant an increasing l value, inducing more photons emitted efficiently into the target dish and consequently

Downloaded from http://iwaponline.com/wst/article-pdf/83/10/2526/892299/wst083102526.pdf
by guest

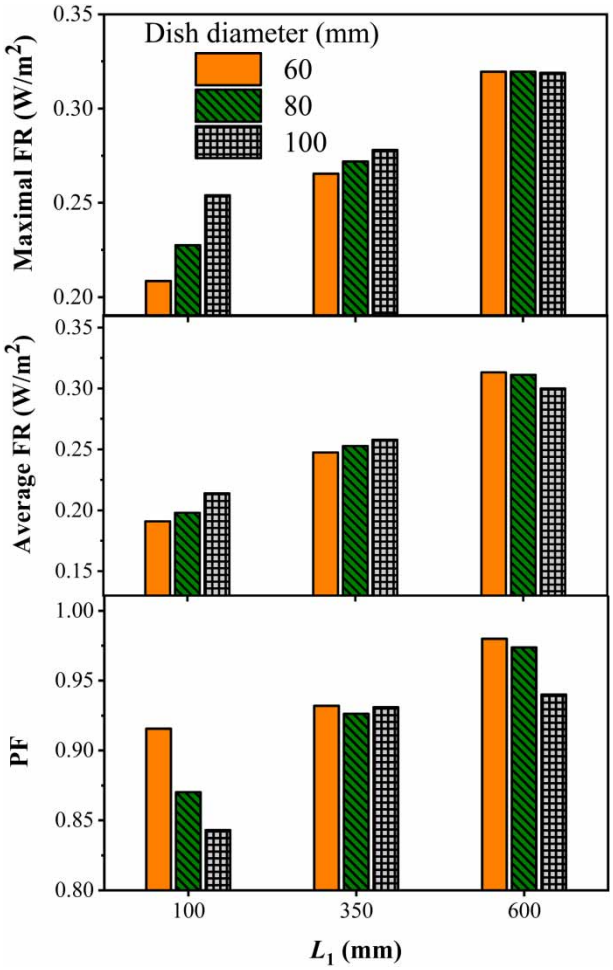

Figure 2 | Simulated FR and PF values on target surfaces induced by single-aperture constrained beams with different distances (L_1) from the UV lamp to the aperture (collimator diameter = 100 mm, and distance between lamp and Petri dish = 900 mm).

increasing the average and maximal FR values. On the other hand, as the α value decreased with the increased L_1, a more centralized beam was irradiated to the central part of the target dish, inducing an increasing PF value.

The size of dishes made almost no difference to FR distributions throughout the QCBAs, which are mainly determined by collimators and UV lamps. The PF and FR values would remain constant with a changing d value in dishes irradiated by completely parallel beams. Thus, the variation of PF and FR values on the upper surface of dishes with the change of d value could reveal the parallelism of the designed QCBA to a certain degree. In QCBAs with $L_1 = 100$ and 350 mm (Figure S3(a) and S3(b)), the maximal FR values appear in the surrounding area, inducing a decrease of average and maximal FRs as the d value decreased from 100 to 60 mm (average FR value decreases by 11% and 4% in Figure S3(a) and S3(b), respectively; maximal FR value decreases by 18% and 5% in Figure S3(a) and S3(b), respectively). In QCBA with $L_1 = 600$ mm (Figure S3(c)), where the FR value at the central point is the maximal one, the maximal FR remains constant and the average FR changes minimally with the change of d values. The point with the maximal FR value shows a gradual transfer towards the central from the surrounding areas, leading the PFs to show different changing trends with the decreasing d values. In Figure S2(a), the PF value increases as d value decreases from 100 to 60 mm; in Figure S2(b), the PF value changes minimally (0.930 ± 0.003) with a decreasing d value; while in Figure S2(c), the PF value increases as d value decreases from 100 to 80 mm, and remains at this level as d value decreases from 80 to 60 mm. Thus, to obtain an appropriate output intensity and parallelism, the designed collimator diameter should be larger than the reactor diameter.

UV beams constrained by multiple successive apertures and cylindrical tube

In QCBAs constrained by a single aperture, there were still a few beams with the α value less than 90° irradiated on target dishes. Figure S5 and Figure 3 show the simulated FR distributions in QCBAs with multiple successive apertures and a cylindrical tube. UV beams constrained by multiple successive apertures or cylindrical tube were more centralized than those from QCBAs with one single aperture. With the same length of collimator (the distance between apertures from top to bottom, or the length of cylindrical tube) and the same L_1 value, beams in the QCBA with two apertures showed slightly larger average and maximal FR and PF values (i.e., 0.164 W/m^2, 0.159 W/m^2, and 0.967 in a 60-mm dish, respectively) than the three-aperture- and the tube-type QCBA.

The tube-type QCBA could be considered as one with infinite multilayer apertures. As the aperture number increased, the proportion of UV beam eliminated by apertures was increased automatically. In Figure S5, the UV beam eliminated by apertures is mainly concentrated in surrounding areas, and the central area changes minimally, inducing that d values have little influence on the FR and PF values in the two-aperture-type QCBA, and in contrast, the FR and PF values in the tube-type QCBA changed obviously with the variation of d values. The PF value (0.875) of the tube-type QCBA with $d = 100$ mm was significantly worse than other values ($\geq$0.928). QCBAs with two successive apertures were enough to produce satisfactory parallel beams. In addition, the construction cost could be

Downloaded from http://iwaponline.com/wst/article-pdf/83/10/2526/892299/wst083102526.pdf
by guest

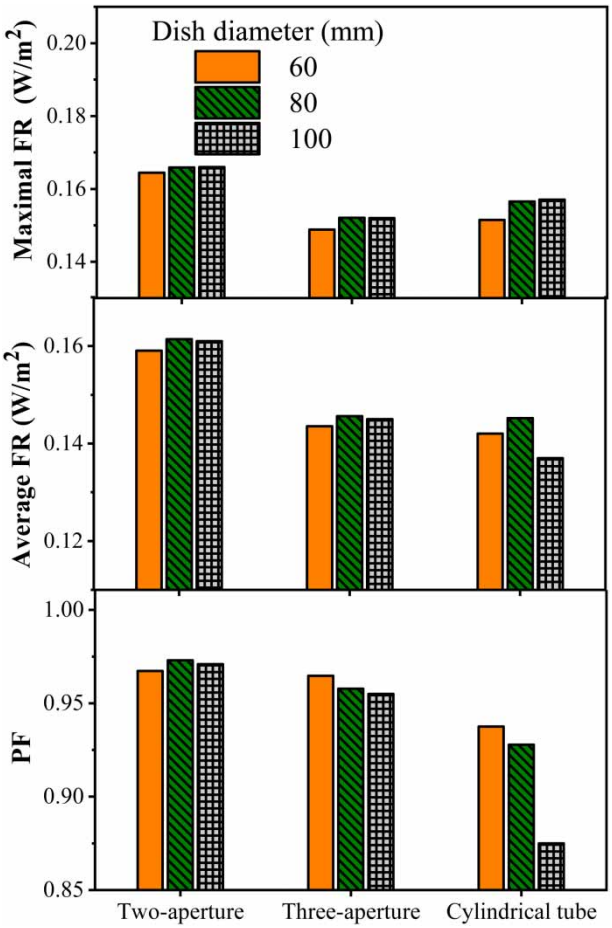

Figure 3 | Simulated FR and PF values on target surfaces induced by multiple successive apertures and cylindrical tube (collimator diameter = 100 mm, distance between lamp and Petri dish = 900 mm, length of collimator = 500 mm, distance between lamp and upper aperture = 100 mm).

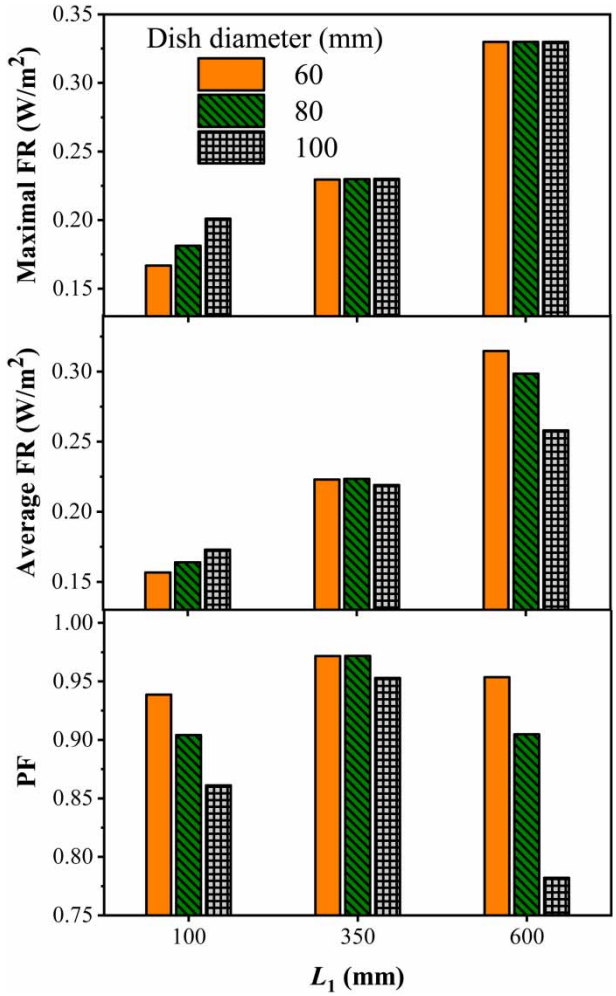

Figure 4 | Simulated FR and PF values on target surfaces in two-aperture-type QCBAs with different distances (L_1) from the UV lamp to the upper aperture (collimator diameter = 100 mm, distance between lamp and Petri dish = 900 mm, distance between each aperture = 250 mm).

reduced by decreasing the number of apertures; the construction of successive apertures was much easier than that of a cylindrical tube, and the dual-aperture structure could also minimize the effect of UV reflection from the collimator walls, which was not involved in this study, especially compared with the cylindrical tube.

To access the effect of aperture position on the FR distributions in dual-aperture QCBAs, simulations of QCBAs with fixed distance (L_2) between each aperture and different L_1 values were performed (results shown in Figure S6 and Figure 4). Although the point with the maximal FR value appeared in different places as L_1 was extended, the PF values in a 60-mm dish were quite high (> 0.93), and the largest value (0.972) in the QCBA was with the L_1 value of 350 mm. The average and maximal FR values in all dishes showed an increasing trend with the increased L_1 value (e.g., from 0.167 to 0.330 W/m^2 and 0.157 to 0.315 W/m^2 for the maximal and average FR values in a 60-mm dish, respectively). It could also be observed that with the two fixed apertures away from the UV lamp, the FR distribution became concentrated, especially in the central area. The maximal FR point transferred to the center from the sides, and the surrounding beam gradually decreased, inducing PF value reduced significantly with an increasing d value. The minimal PF value was even <0.80, which occurred in a 100-mm dish with $L_1 = 600$ mm. These results were quite similar to those from the single-aperture QCBAs in Figure S3 and Figure 2.

Figure S7 and Figure 5 show the effect of L_2 values on the FR distributions in two-aperture-type QCBAs. In these experiments, the upper aperture was fixed at 100 mm

Downloaded from http://iwaponline.com/wst/article-pdf/83/10/2526/892299/wst083102526.pdf
by guest

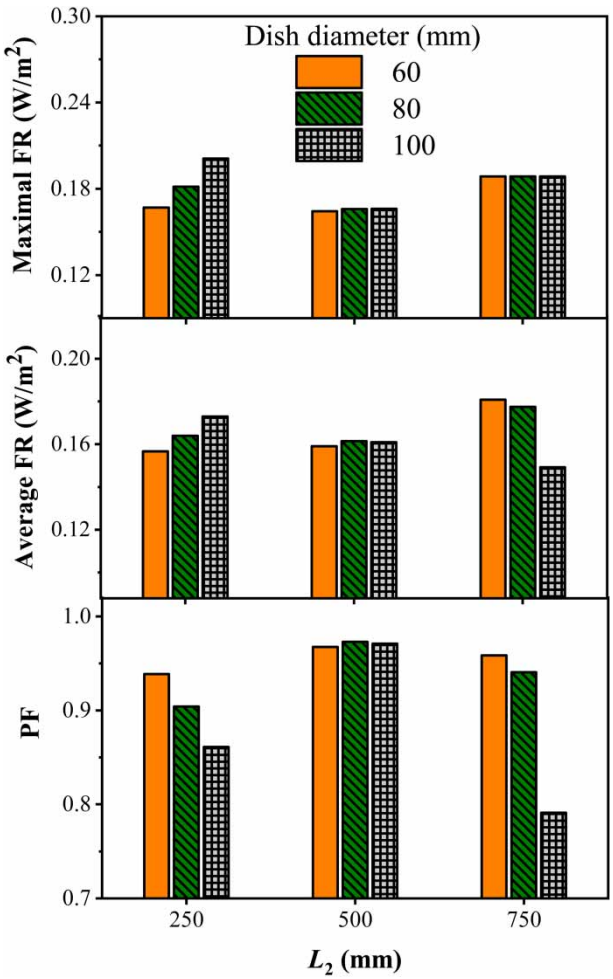

Figure 5 | Simulated FR and PF values on target surfaces in two-aperture QCBAs with different distances (L_2) between apertures (collimator diameter = 100 mm, distance between lamp and Petri dish = 900 mm, distance between lamp and upper aperture = 100 mm).

away from the lamp, and the lower aperture was set at 250, 500, or 750 mm away from the upper one. A trend of UV beam from dispersion to concentration was also observed as L_2 increased. A weakening of UV beam intensity occurs in the central area when $l_2 = 250$ mm (Figure S7(a)), while the maximal FR value appears at the central point, and the UV irradiation in the margin area is negligible when $l_2 = 750$ mm (Figure S6(c)). Despite these variations, the change of average FR (0.156–0.181 W/m^2), maximal FR (0.164–0.189 W/m^2), and PF (0.938–0.967) values in a 60-mm dish with the increased L_2 was slight; the largest average and maximal FR value occurred in the QCBA when $L_2 = 750$ mm, and the largest PF value was equal to 0.967 when $L_2 = 500$ mm.

Effect of lamp type, number, and pattern

Besides the geometrical character of QCBA, the type, number and position of the UV lamp would also affect the intensity and parallelism of the UV beam irradiated in the selected dish. Figure S8 shows the effect of different irradiations on the FR distribution. According to the DO model, the UV lamp irradiation had little effect on the parallelism of UV beam, as is shown in Figure S8. The UV intensity in selected dishes was directly proportional to the irradiation of lamp, and the optimized geometry would remain constant with a changing irradiation of selected lamps. As shown in Equation (2), the lamp irradiation was directly proportional to the UV output power and inversely proportional to the lamp surface area (an assumption was made in the DO model that UV beams were emitted from the lamp sleeve; this assumption would obviously simplify the calculation and have little effect on the computational accuracy). Thus, a compact lamp with a high UV output power and a short arc length is recommended in the construction of QCBAs. The effect of UV lamp type on the intensity and parallelism of QCBA was relatively simple and clear. This study was mainly focused on the optimization of QCBA with given lamps, and the brand and model of UV lamps were not further discussed. In fact, the power of the selected model lamp was quite low (10 W), leading the simulated FR value in this study to be relatively low (Antoniou & Andersen 2015; Qiang *et al.* 2015; Rozas *et al.* 2016).

The average FR values in the simulated QCBAs above ranged from 0.142 to 0.315 W/m^2. To achieve a UV dose of 1,000 mJ/cm^2, which is typical in the study of UV photochemical processes and UV-based advanced oxidation processes (AOPs) (Lian *et al.* 2015; Kong *et al.* 2016), the irradiation time should be set at several hours, making the studies time-consuming and impractical. To increase the UV intensity in QCBA, multiple-lamp configurations were investigated in this study. From Figure S9 and Figure 6, increasing the number of lamps had minimal effect on the UV parallelism in the target dish compared with that in a single-lamp QCBA, but obviously enhanced the maximal and average FR values, which were approximately proportional to the number of UV lamps. The multiple-lamp pattern with lamps adjacent in the middle over the collimator hole showed a similar PF value to the pattern of lamps evenly arranged along the diameter of the target area, while the maximal and average FR values in the former were a little larger than those in the latter, for both QCBAs with two or three lamps. QCBAs with multiple

Downloaded from http://iwaponline.com/wst/article-pdf/83/10/2526/892299/wst083102526.pdf
by guest

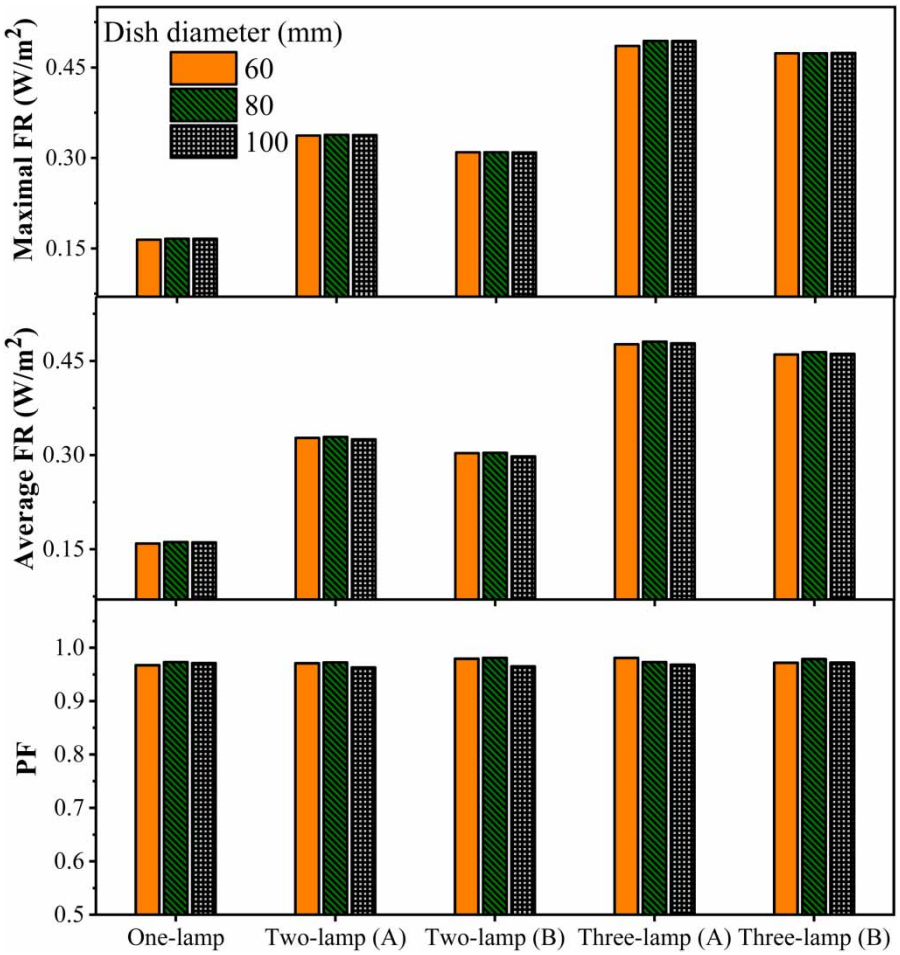

Figure 6 | Simulated FR and PF values on target surfaces in two-aperture QCBAs with different lamp number. (A) pattern with lamps adjacent in the middle over the collimator hole; (B) pattern of lamps evenly arranged along the diameter of the target area (collimator diameter = 100 mm, distance between lamp and Petri dish = 900 mm, distance between each aperture = 500 mm, distance between lamp and upper aperture = 100 mm).

lamps were favorable to increase the UV output power, and had a nearly negligible loss of parallelism.

Discussion on potential applications

According to the simulations above, an actual QCBA (Figure S2) was constructed to verify the potential application. The detailed parameters were set as follows: two successive apertures, with a BOS-1T5 UVC lamp (10 W, 30% UVC efficiency); $D = 100$ mm, $L_1 = 100$ mm, $L_2 = 500$ mm, and $L = 900$ mm. Figure 7 shows the simulated and experimental FR distribution, which agree very well with each other. The simulated maximal and average FR, and PF values in a 60-mm dish were 0.159 and 0.164 W/m^2, and 0.967, respectively; while the values in the experimental QCBA were 0.163 and 0.167 W/m^2, and 0.976, respectively. The experimental results were a little higher than the simulated ones, which was possibly induced by the fluctuation of UV lamp output and complexity in the actual QCBA. Bolton *et al.* (Bolton & Stefan 2002; Bolton & Linden 2003) suggested that the PF value in a well-designed QCBA should be > 0.9, and in this study, the PF values in the experimental QCBA with different d values were both superior to this suggestion.

CONCLUSIONS

This study simulated the FR distributions in QCBAs using CFD models, and proposed an optimized construction configuration for QCBAs with given UV lamps. Based on the simulation results, the main conclusions are as follows.

Downloaded from http://iwaponline.com/wst/article-pdf/83/10/2526/892299/wst083102526.pdf
by guest

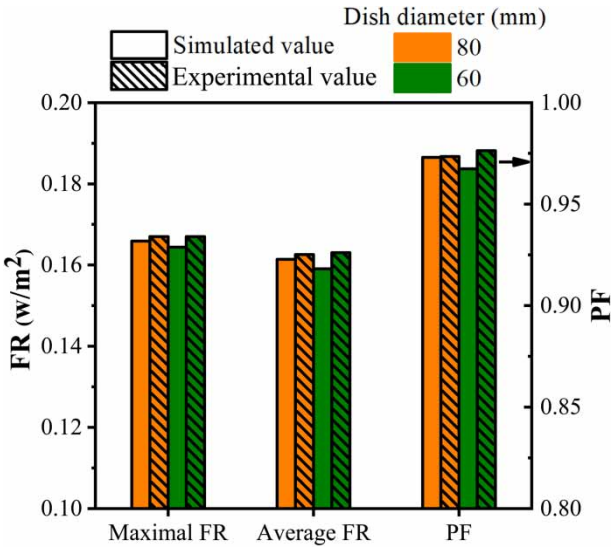

Figure 7 | Comparison of the experimental and simulated FR distribution in the constructed QCBA (two successive apertures, with a BOS-1T5 UVC lamp; collimator diameter = 100 mm, distances from the UV lamp to the upper aperture = 100 mm, distance between each aperture = 500 mm, and distance between lamp and Petri dish = 900 mm).

UV beams constrained by a single aperture were possessed of a certain parallelism (PF > 0.84); with the increase of the distance from the UV lamp to the upper aperture, both PF and FR values increased in QCBAs with a single aperture.

QCBAs with two successive apertures produced satisfactory parallel beams; when the distance between the lamp and the upper end of the collimator increased, the FR distribution in QCBAs with two fixed-interval apertures became concentrated, especially in the marginal area, and this concentration trend could be also observed as the interval distance between apertures increased.

QCBAs with multiple lamps were favorable to increase the UV output power, and with a nearly negligible loss of parallelism. The maximal and average FR values in QCBAs with lamps adjacent in the middle over the collimator hole were a little larger than those in QCBAs with the pattern of lamps evenly arranged along the diameter of the target area.

The potential application of CFD simulated QCBAs was verified with an actual QCBA. The experimental maximal and average FR and PF values in a 60-mm dish were 0.159 and 0.164 W/m^2, and 0.967, respectively, which agreed very well with the simulated results.

This study would help in the normalization of QCBA construction, and promote the practical application of UV disinfection and UV-based technology in water and drinking water treatment.

ACKNOWLEDGEMENTS

This study was funded by the National Natural Science Foundation of China (51808268) and the Natural Science Foundation of Jiangxi Province (20171BAB216040, GJJ160658).

DATA AVAILABILITY STATEMENT

All relevant data are included in the paper or its Supplementary Information.

REFERENCES

Antoniou, M. G. & Andersen, H. R. 2015 Comparison of UVC/$S_2O_8^{2-}$ with UVC/H_2O_2 in terms of efficiency and cost for the removal of micropollutants from groundwater. *Chemosphere* **119**, S81–S88.

Ao, X. W., Chen, Z. Y., Li, S. M., Li, C., Lu, Z. D. & Sun, W. J. 2020 The impact of UV treatment on microbial control and DBPs formation in full-scale drinking water systems in northern China. *Journal of Environmental Sciences* **87**, 398–410.

Baeza, C. & Knappe, D. R. U. 2011 Transformation kinetics of biochemically active compounds in low-pressure UV photolysis and UV/H_2O_2 advanced oxidation processes. *Water Research* **45**, 4531–4543.

Bolton, J. R. & Linden, K. G. 2003 Standardization of methods for fluence (UV dose) determination in bench-scale UV experiments. *Journal of Environmental Engineering* **129** (3), 209–215.

Bolton, J. R. & Stefan, M. I. 2002 Fundamental photochemical approach to the concepts of fluence (UV dose) and electrical energy efficiency in photochemical degradation reactions. *Research on Chemical Intermediates* **28**, 857–870.

Bolton, J. R., Beck, S. E. & Linden, K. G. 2015 Protocol for the determination of fluence (UV dose) using a low-pressure or low-pressure high-output UV lamp in bench-scale collimated beam ultraviolet experiments. *IUVA News* **17**, 11–16.

General Administration of Quality Supervision, Inspection and Quarantine of the People's Republic of China (GAQSIQ) 2005 *Ultraviolet (UV) Disinfection Equipment for Municipal Water and Wastewater Treatment. (GB/T19837-2005)*.

Gholamalizadeh, E. & Kim, M. H. 2014 Three-dimensional CFD analysis for simulating the greenhouse effect in solar chimney power plants using a two-band radiation model. *Renewable Energy* **63**, 498–506.

Jefferson, B., Jarvis, P., Bhagianathan, G. K., Smith, H., Autin, O., Goslan, E. H., MacAdam, J. & Carra, I. 2016 Effect of elevated UV dose and alkalinity on metaldehyde removal and THM formation with UV/TiO_2 and UV/H_2O_2. *Chemical Engineering Journal* **288**, 359–367.

Downloaded from http://iwaponline.com/wst/article-pdf/83/10/2526/892299/wst083102526.pdf
by guest

Jin, J., El-Din, M. G. & Bolton, J. R. 2011 Assessment of the UV/chlorine process as an advanced oxidation process. *Water Research* **45** (4), 1890–1896.

Ke, Q. S., Craik, S. A., El-Din, M. G. & Bolton, J. R. 2009 Development of a protocol for the determination of the ultraviolet sensitivity of microorganisms suspended in air. *Aerosol Science and Technology* **43**, 284–289.

Kong, X. J., Jiang, J., Ma, J., Yang, Y., Liu, W. L. & Liu, Y. L. 2016 Degradation of atrazine by UV/chlorine: efficiency, influencing factors, and products. *Water Research* **90**, 15–23.

Lebedev, N., Grachev, V., Pliamina, O. V., Lebedev, O., Lukichyova, D., Doilnitsyn, V., Akatov, A. & Leonov, L. 2019 Testing combined application of ultraviolet and ultrasonic disinfection of wastewater. *International Journal of Mechanical Engineering and Technology* **10** (3), 1566–1573.

Li, W. T., Li, M. K., Bolton, J. R. & Qiang, Z. M. 2016 Configuration optimization of UV reactors for water disinfection with computational fluid dynamics: feasibility of using particle minimum UV dose as a performance indicator. *Chemical Engineering Journal* **306**, 1–8.

Li, W. T., Li, M. K., Bolton, J. R., Qu, J. H. & Qiang, Z. M. 2017 Impact of inner-wall reflection on UV reactor performance as evaluated by using computational fluid dynamics: the role of diffuse reflection. *Water Research* **109**, 382–388.

Lian, J. F., Qiang, Z. M., Li, M. K., Bolton, J. R. & Qu, J. H. 2015 UV photolysis kinetics of sulfonamides in aqueous solution based on optimized fluence quantification. *Water Research* **75**, 43–50.

Ministry of Housing and Urban-Rural Development of the People's Republic of China (MOHURD) 2006 *Code for Design of Outdoor Wastewater Engineering (GB50014-2006)*.

Pan, Y. P., Tian, X. Q., Zhang, B. F., Zhu, Z. F., Pan, H. C., Rahman, M. M. & Leng, J. X. 2020 Numerical verification for a new type of UV disinfection reactor. *Ain Shams Engineering Journal* **11**, 1191–1200.

Qiang, Z. M., Li, W. T., Li, M. K., Bolton, J. R. & Qu, J. H. 2015 Inspection of feasible calibration conditions for UV radiometer detectors with the KI/KIO_3 actinometer. *Photochemistry and Photobiology* **91** (1), 68–73.

Qualls, R. G. & Johnson, J. D. 1983 Bioassay and dose measurement in UV disinfection. *Applied and Environmental Microbiology* **45** (3), 872–877.

Rozas, O., Vidal, C., Baeza, C., Jardim, W. F., Rossner, A. & Mansilla, H. D. 2016 Organic micropollutants (OMPs) in natural waters: oxidation by UV/H_2O_2 treatment and toxicity assessment. *Water Research* **98**, 109–118.

Schmalwieser, A. W., Wright, H., Cabaj, A., Mark, H., Erin, M. & Günther, S. 2014 Aging of low-pressure amalgam lamps and UV dose delivery. *Journal of Environmental Engineering and Science* **9** (2), 113–124.

Sozzi, D. A. & Taghipour, F. 2006 UV reactor performance modeling by Eulerian and Lagrangian methods. *Environmental Science & Technology* **40** (5), 1609–1615.

Spiliotopoulou, A., Hansen, K. M. S. & Andersen, H. R. 2015 Secondary formation of disinfection by-products by UV treatment of swimming pool water. *Science of the Total Environment* **520**, 96–105.

Stefan, M. I. & Bolton, J. R. 2005 Fundamental approach to the fluence-based kinetic and electrical energy efficiency parameters in photochemical degradation reactions: polychromatic light. *Journal of Environmental Engineering and Science* **4** (S1), S13–S18.

Sultan, T. 2016 Numerical study of the effects of lamp configuration and reactor wall roughness in an open channel water disinfection UV reactor. *Chemosphere* **155**, 170–179.

Zhang, Z. G., Li, B. X., Li, N., Sardar, M. F., Song, T. T., Zhu, C. X., Lv, X. W. & Li, H. N. 2019 Effects of UV disinfection on phenotypes and genotypes of antibiotic-resistant bacteria in secondary effluent from a municipal wastewater treatment plant. *Water Research* **157**, 546–554.

First received 28 December 2020; accepted in revised form 29 March 2021. Available online 9 April 2021

Downloaded from http://iwaponline.com/wst/article-pdf/83/10/2526/892299/wst083102526.pdf
by guest